Supplemental Materials

Participants

A total of 214 patients with paediatric mild traumatic brain injury (pmTBI) were consecutively recruited from local Emergency Room and Urgent Care departments along with 186 statistically matched (sex and age) healthy controls (HC). Fourteen individuals (5 pmTBI and 9 HC) withdrew from the study prior to collection of diffusion magnetic resonance imaging (dMRI) data during their sub-acute (SA) visit. No attempt was made to bring these participants back for a second visit. This resulted in a potential sample of 209 pmTBI and 177 HC for return appointments prior to determining motion outliers or identifying issues with the data acquisition. From this subset, study attrition occurred for 39 pmTBI (81.3% retention) and 8 HC (95.5% retention), while an additional 8 pmTBI and 1 HC where unable complete study procedures due to the COVID-19 pandemic. This resulted in 162 pmTBI and 168 HC eligible for scanning during their early chronic (EC) visit. Six HC were excluded (3 drug use, 1 new psychiatric diagnosis) or contraindications to dMRI (2 new braces). Similarly, 8 pmTBI had emerging contraindications (5 new braces, 3 medical conditions) and 2 declined the MRI portion of the experiment. Motion outliers (three times the interquartile range) were determined by combining all available SA and EC data within each cohort. A total of 1 pmTBI and 1 HC were identified as motion outliers on their SA dMRI scans, with an additional 3 HC identified as motion outliers on their EC dMRI scans. Additionally, issues with data acquisition (e.g., incorrect phase encoding directions) were identified in 4 pmTBI and 3 HC scans from the SA visit, with an additional 4 problematic HC acquisitions from the EC visit. The final sample with usable dMRI data included 204 pmTBI (83 females; age 14.5±2.9; 7.4±2.2 days post-injury) and 173 HC (73 females; age 14.2±2.8) for the SA visit. In addition, 152 pmTBI (63 females; 130.9±14.5 days post-injury; 124.0±14.6 days between visits; 81.3% retention

without study excludes) and 155 HC (65 females; 124.2±15.7 days between visits; 95.5% retention without study excludes) were included at the EC visit.

Common Data Element Measures

A urine screen for amphetamines, cocaine, marijuana, methamphetamines, opiates, phencyclidine, benzodiazepines, barbiturates, methadone and methylenedioxy-methamphetamine use was administered to all participants, with a positive screen resulting in exclusion.

The cognitive battery included tests of premorbid cognitive ability (Wide Range Achievement Test [WRAT4])[1], a shortened measure of effort (Test of Memory Malingering [TOMMe10])[2], and selected tests from the Delis-Kaplan Executive Function System (DKEFS)[3], the Hopkins Verbal Learning Test-Revised (HVLT), and Wechsler Intelligence Scales depending on initial age at assessment. The Wechsler Adult Intelligence Scale–IV (WAIS-IV)[4] was used for participants 16-18 years old at enrolment whereas the Wechsler Intelligence Scale for Children–V (WISC-V)[5] was used for participants 8-15 years old at enrolment. Composite measures of attention (DKEFS colour-word interference conditions 1-3), processing speed (WAIS-IV/WISC-V digit symbol coding and symbol search), working memory (WISC-V/WAIS-IV digit span backwards trial), executive function (DKEFS trail making test condition 4, verbal fluency, colour-word interference condition 4) and long-term memory recall (HVLT Delay) were compiled to create specific cognitive domains.

Categorical representations of loss of consciousness (LOC) and post-traumatic amnesia (PTA) were used due to their superior psychometric properties relative to a continuous measurement [6]. The 5P risk score [7] was calculated with minor modifications based on available clinical data. Standard calculations included age, sex, prior concussion history and symptom duration, physician-diagnosed migraine history, as well as headaches, sensitivity to noise and

fatigue on the Post-Concussion Symptom Inventory (PCSI) parent form. Modifications in the current study included use of a tandem gait task rather than the recommended mBESS tandem stance, and the "answers questions more slowly" from the PCSI parent form rather than from the Acute Concussion Evaluation. A severity score was calculated for each factor and then summed for a total risk score using recommended criteria [7].

The PCSI was modified in the following ways with author permission: 1) the version of the PCSI for 13-18 year old was also utilized for 12 year old participants, and 2) all references to an injury were removed from both questionnaires and instructions to avoid bias in HC. The retrospective (i.e., one month prior to initial visit) and SA (day of initial visit) reporting instructions were also specified in the revised version. All summary scores from the PCSI were normalized into percentage values given that different scales were administered to older (ages 12-18) and younger children (ages 8-11).

MR Imaging Parameters

All participants were scanned on a 3T TrioTim system (Siemens; Erlangen, Germany) with a 32-channel head coil. A high resolution 5-echo Magnetization Prepared Rapid Acquisition Gradient Echo (MPRAGE) T_1–weighted [repetition time (TR)=2530 ms; echo times (TE)=1.64, 3.50, 5.36, 7.22, 9.08 ms; inversion time (TI)=1200 ms; flip angle=7°; number of excitations (NEX)=1; slice thickness=1 mm; field of view (FOV)=256 mm; matrix size=256 x 256; isotropic voxels=1 mm^3] was collected in addition to a T_2–weighted sequence [TR=15500 ms; TE=77 ms; flip angle=155°; NEX=1; slice thickness=1.5mm; FOV=220 mm; matrix size=192 x 192; voxel size=1.15 x 1.1.5 x 1.5 mm]. SWI data were collected using one T_2-weighted gradient echo sequence [TR = 28 ms; TE = 20.0 ms; flip angle = 15°; NEX = 1; slice thickness = 1.5 mm; FOV = 192 × 256; matrix size = 192 × 256; voxel size = 1.00 × 1.00 × 1.50 mm]. Finally, FLAIR data

were also collected [TR = 10380 ms; TE = 88.0 ms; TI = 2500 ms; flip angle = 140°; NEX = 1; slice thickness = 3 mm; FOV = 256 mm; matrix size = 320 × 320; voxel size = 0.80 × 0.80 × 3.00 mm]. Foam padding was used to limit head motion on all scan sequences.

The dMRI data were collected across 4 runs, with reversed phase encoding direction distributed evenly across runs (A→P; P→A). Gradient directions at each shell were selected based on previously published guidelines [8,9] and were uniformly distributed over an electrostatic sphere using the CAMINO software package [10,11]. Each participant's mean, unwarped b0 image from TOPUP was registered to their T_1-weighted image using an affine transformation, with T_1 images subsequently normalized to Talairach space (AFNI TT_N27) using a non-linear transformation (AFNI 3dQwarp). Both matrices were concatenated to bring DTI scalars into stereotaxic space. All DTI and volume fraction estimates were spatially normalized using the same concatenated matrices and blurred using a 6 mm FWHM Gaussian kernel.

Cellular microstructure was investigated using the standard NODDI algorithm [12] (MATLAB v2020a) using fixed rates for isotropic (3.0×10^{-3} mm^2/s), intracellular (1.7×10^{-3} mm^2/s) and extracellular (1.7×10^{-3} mm^2/s) diffusivity, and a non-linear gradient descent to determine the maximum likelihood of the parameters with a Gaussian noise model (variance = 1). A more biologically informed model was also run using the python-based Microstructure Diffusion Toolbox (MDT; v1.2.6; https://mdt-toolbox.readthedocs.io) using the gradient-free Powell conjugate-direction algorithm and the cascade initialization option with an offset Gaussian noise model and automatically estimated noise variance [13]. Separate models were included in which isotropic diffusivity remain fixed (3.0×10^{-3} mm^2/s) but parallel diffusivities were varied for both white matter (WM; intracellular = 1.7×10^{-3} mm^2/s; extracellular constrained to be less than $1.7\times10^{-}$

^{3} mm^2/s) and grey matter (GM; intracellular = 1.2×10^{-3} mm^2/s; extracellular unconstrained) based on biologically informed estimates of diffusivities [14-16].

To derive tissue specific models, an individual participant's T_1-weighted data were first analysed with the Statistical Parametric Mapping segmentation algorithm. Next, each voxel was designated as either GM, WM or cerebral spinal fluid based on the highest maximum probability value across all three tissue classes. The two biologically informed MDT models were then run separately for each participant's dMRI data and the data combined across the different tissue types based on the aligned T_1 segmentation results prior to smoothing. Model parameter selection is further complicated in deep GM structures such as the thalamus and basal ganglia since they represent a mixture of both GM and WM [16]. In the current study, all deep GM structures were modelled using our GM parameters.

Statistical Analysis

All demographic and clinical analyses were limited to participants with good diffusion data for consistency. Demographic data were evaluated between groups using chi-square (sex, previous history of concussions and handedness, parental education, self-reported Tanner stage of development) and Mann-Whitney U (age at injury) non-parametric tests. Primary and secondary clinical data were assessed using age at injury as a covariate, as well as retrospective ratings when applicable. Clinical analyses were conducted with either generalized linear models (GLM; Group effect only) or generalized estimating equations (GEE; Group and time effect), using Gaussian, gamma or negative binomial distributions based on data type and Information Criteria modelling fits. GEE models were also used to examine the relationship between clinical gold standards of injury severity and dMRI abnormalities. Primary clinical (0.05/3 = 0.017) and neuropsychological (0.05/2 = 0.025) tests were Bonferroni-corrected for overall number of comparisons, whereas

secondary tests were Bonferroni-corrected within each respective domain. Voxelwise dMRI results were corrected for family-wise error using parametric ($p \leq 0.001$) and minimum volume thresholds (fractional anisotropy [FA]=568 µl; mean diffusivity [MD]=1184 µl; intracellular volume fraction [V_{ic}]=896 µl; isotropic volume fraction [V_{iso}]=1016 µl; orientation dispersion index [ODI]=768 µl) based on results from 10,000 Monte Carlo simulations and spherical autocorrelation estimates [17].

Classification Analyses

Finally, a Random forests (RF) approach was used to classify pmTBI from HC. RF is a supervised ensemble learning algorithm [18,19] in which multiple classification trees (a "forest") are fit on bootstrapped samples of the original data. Each tree partitions the data based on a random subset of predictor variables to optimally separate diagnostic categories. RF does not have distributional model assumptions and automatically employs external cross-validation by predicting a patient diagnosis based on trees estimated without that patient. RF provides a measure of variable importance for prediction accuracy, as well the marginal probability of group identity for values of each variable, and the bootstrap aggregating technique keeps RF from overfitting. The variable importance (VIMP, Breiman-Cutler permutation importance) metric is the reduction of prediction accuracy for an external validation set comparing decision trees with the feature compared to trees without that feature. RF was performed in R software (4.1.1) using package "randomForestSRC" function "rfsrc" with 1000 trees [20,21].

Results

Clinical, Neuropsychological and Behavioural Analyses

Ten pmTBI and four HC failed TOMMe10, the measure of effort (Score < 8). One pmTBI was excluded from further analyses after the inspection of their scores on neuropsychological measures indicated sub-optimal performance (greater than 1.5 standard deviations below the mean) for other cognitive domains on traditional paper and pencil testing. All other individual performed within normal limits on other cognitive domains and generally had consistent scores across SA and EC visits and were retained for analyses.

Unique MDT Findings for V_{ic}

The MDT model also indicated multiple other unique areas of increased V_{ic} for pmTBI relative HC in both GM and WM (Figure 4F). Specifically, increased V_{ic} was observed in the right (BAs 8/9; 1571 µl) and left (BA 9; 1063 µl) middle/superior frontal gyrus right middle frontal gyrus (BAs 8/9/10; 1862 µl), right (BAs 11/47; 3867 µl) and left (BAs 11/47; 1131 µl) inferior frontal gyrus with the right encompassing adjacent uncinate fasciculus, right posterior insula and superior temporal gyrus (BAs 13/22/41; 4954 µl), right mid-insula (BAs 6/13/44; 974 µl), grey/white junctions of the left inferior/middle temporal gyrus and inferior/middle longitudinal fasciculi (BAs 20/21; 6122 µl), right sensorimotor cortex (BAs 3/4/6; 947 µl), left postcentral gyrus extending into inferior parietal lobule (BA 40/41; 1372 µl), left supramarginal gyrus (BAs 13/22/40; 1385 µl), right inferior parietal lobe (BA 40; 1605 µl), bilateral visual cortex/cuneus (BAs 17/18/23/30; 4155 µl), left thalamus extending into the parahippocampal gyrus (BAs 27/30; 1018 µl), right thalamus extending to lingual gyrus (BAs 18/19/30; 1872 µl), and Lobules I-IV of the cerebellum (1534 µl).

Reproducibility and Effect Size Estimates

Cohen's d effect sizes with variance pooled across groups were calculated by averaging SA and EC visit data when it was available or by using single visit data (S-Figures 5-8).

Additional cross-validation analyses were conducted to examine the reproducibility of our dMRI findings in smaller sample sizes. Specifically, pmTBI and HC were randomly sampled without replacement at sample sizes of either 50%, 60% or 70% of total sample size, and group-wise tests repeated. Voxels exhibiting a main effect of group at uncorrected *p* values of 0.01 (tests repeated to determine adequate correction levels) were summed and then divided by the number of iterations (N=300 at each sample size) to form a voxelwise percentage value of reproducibility. Due to largely duplicative results with NODDI, only results for DTI (S-Figure 9) and biologically informed MDT volume fraction estimates (Figure 6) are presented for the reproducibility analyses.

References

1. Wilkinson GS, Robertson GJ. *WRAT 4: Wide range achievement test; professional manual*. Psychological Assessment Resources, Incorporated; 2006.
2. Denning JH. The efficiency and accuracy of the Test of Memory Malingering trial 1, errors on the first 10 items of the test of memory malingering, and five embedded measures in predicting invalid test performance. *Arch Clin Neuropsychol.* 2012;27(4):417-432.
3. Delis DC, Kaplan E, Kramer JH. *Delis-Kaplan executive function system (D-KEFS)*. Psychological Corporation; 2001.
4. Wechsler D. *Wechsler adult intelligence scale-fourth*. San Antonio: Pearson; 2008.
5. Wechsler D. Wechsler intelligence scale for children – Fifth edition (WISC-V): Technical and interpretive manual. 2014. Bloomington, MN: Pearson Clinical Assessment.
6. Hergert DC, Sicard V, Stephenson DD, et al. Test-Retest Reliability of a Semi-Structured Interview to Aid in Pediatric Traumatic Brain Injury Diagnosis. *J Int Neuropsychol Soc.* 2021;1-13.
7. Zemek R, Barrowman N, Freedman SB, et al. Clinical risk score for persistent postconcussion symptoms among children with acute concussion in the ED. *JAMA.* 2016;315(10):1014-1025.
8. Jones DK, Williams SC, Gasston D, Horsfield MA, Simmons A, Howard R. Isotropic resolution diffusion tensor imaging with whole brain acquisition in a clinically acceptable time. *Hum Brain Mapp.* 2002;15(4):216-230.
9. Skare S, Li T, Nordell B, Ingvar M. Noise considerations in the determination of diffusion tensor anisotropy. *Magn Reson Imaging.* 2000;18(6):659-669.
10. Jansons KM, Alexander DC. Persistent angular structure: new insights from diffusion magnetic resonance imaging data. *Inverse Problems.* 2003;19(5):1031.
11. Jones DK, Horsfield MA, Simmons A. Optimal strategies for measuring diffusion in anisotropic systems by magnetic resonance imaging. *Magn Reson Med.* 1999;42(3):515-525.
12. Zhang H, Schneider T, Wheeler-Kingshott CA, Alexander DC. NODDI: practical in vivo neurite orientation dispersion and density imaging of the human brain. *Neuroimage.* 2012;61(4):1000-1016.
13. Harms RL, Fritz FJ, Tobisch A, Goebel R, Roebroeck A. Robust and fast nonlinear optimization of diffusion MRI microstructure models. *Neuroimage.* 2017;155:82-96.
14. Guerrero JM, Adluru N, Bendlin BB, et al. Optimizing the intrinsic parallel diffusivity in NODDI: An extensive empirical evaluation. *PLoS One.* 2019;14(9):e0217118.
15. Jelescu IO, Budde MD. Design and validation of diffusion MRI models of white matter. *Front Phys.* 2017;5:61.
16. Jelescu IO, Palombo M, Bagnato F, Schilling KG. Challenges for biophysical modeling of microstructure. *J Neurosci Methods.* 2020;344:108861.
17. Cox R, Chen G, Glen DR, Reynolds RC, Taylor PA. FMRI Clustering in AFNI: False Positive Rates Redux. *Brain Connectivity.* 2017;7(3):152-171.
18. Breiman L. Statistical modeling: The two cultures. *Statistical Science.* 2001;16(3):199-231.
19. Breiman L. Random forests. *Machine learning.* 2001;45(1):5-32.
20. randomForestSRC: Fast Unified Random Forests for Survival, Regression, and Classification (https://cran.r-project.org/package=randomForestSRC) [computer program]. The Comprehensive R Archive Network; 2021.
21. Ishwaran H, Malley JD. Synthetic learning machines. *BioData mining.* 2014;7(1):1-12.

S-Table 1: Primary and secondary clinical and neurocognitive measures.

Instrument	Measured domain	Status	Rater	Visit
Demographics				
NewMAP TBI	Self-reported TBI history	Secondary	C & P	R, SA, EC
Tanner Stage of Development	Pubertal development	Secondary	C	SA & EC
ASSIST	Use of alcohol and other drugs	Secondary	C	SA & EC
BSI-18	Parental psychopathology	Secondary	P	SA & EC
Clinical Domain				
PCSI	Post-concussive symptoms	Primary	C	R, SA, EC
PROMIS-Sleep	Sleep disturbance	Secondary	C	R, SA, EC
PROMIS-Anxiety	Anxiety symptoms	Secondary	C	R, SA, EC
PROMIS-Depression	Depressive symptoms	Secondary	C	R, SA, EC
Pain scale	Pain	Secondary	C	R, SA, EC
HIT-6	Headache symptoms	Secondary	C	R, SA, EC
CBQ	Family conflict	Primary	C	R, SA, EC
SDQ	Behavioural screening for psychological attributes	Secondary	P	R & EC
PedsQL	Health-related quality of life	Primary	C	R & EC
GOS-E	Functional outcome	Secondary	C & P	SA & EC
Cognitive Domain				
TOMMe10	Measure of effort	Secondary	C	SA & EC
WRAT-4	Premorbid reading ability	Secondary	C	SA & EC
DKEFS Colour-Word interference Cond 1-3	Attention	Primary	C	SA & EC
WAIS-IV/WISC-V Coding and Symbol Search	Processing speed	Primary	C	SA & EC
WISC-V/WAIS-IV Digit Span Backwards	Working memory	Secondary	C	SA & EC
DKEFS Trail Making Test Cond 4, Verbal Fluency, Colour-Word interference Cond 4	Executive function	Secondary	C	SA & EC
HVLT Delayed Recall	Long Term Memory Recall	Secondary	C	SA & EC

Notes: Instrument-- NewMAP TBI: New Mexico Assessment of Pediatric TBI, ASSIST: The Alcohol, Smoking and Substance Involvement Screening Test, BSI: Brief Symptom Inventory-18, PCSI: Post-Concussion Symptom Inventory, PROMIS: Patient-Reported Outcomes Measurement Information System, HIT-6: Headache Impact Test, CBQ: Conflict Behavior Questionnaire, SDQ: Strengths and Difficulties Questionnaire, PedsQL: Pediatric Quality of Life Inventory, GOS-E: Glasgow Outcome Scale Extended, TOMMe10: Test of Memory Malingering, WRAT-4: Wide Range Achievement Test, DKEFS: Delis-Kaplan Executive Function System, WAIS-IV: Wechsler Adult Intelligence Scale–IV, WISC-V: Wechsler Intelligence Scale for Children–V, HVLT: Hopkins Verbal Learning Test; Rater—C: child, P: parent; Visit—R: retrospective, SA: sub-acute, EC: early chronic.

S-Table 2: Demographics and Injury Characteristic Data

	SA pmTBI (N=204)	SA HC (N=173)
Age	14.75(12.63-16.79)	14.25(12.17-16.58)
Sex (% Female)	40.69%	42.20%
Tanner Stage of Development	4(3-4)	4(2-4)
Parent BSI-18*	2(1-6)	1(0-4)
Parent Education (ISCED Category)*	5(3-6)	6(5-7)
pmTBI Hx*	17.16%	6.94%
Injury Characteristics		
Sport- or Recreation-related	57.14%	-
Loss of Consciousness	35.29%	-
Post-Trauma Amnesia	33.66%	-
Mechanism of Injury		
Struck by Object	15.27%	-
Struck by Person	19.70%	-
Fall	26.11%	-
MVC	27.09%	-
Assault	6.40%	-
Bicycle	4.93%	-
Other	0.49%	-

Notes: SA=sub-acute; EC=early chronic; HC=healthy control; pmTBI=paediatric mild traumatic brain injury; BSI=Brief Symptom Inventory-18; ISCED=International Standard Classification of Education; MVC=motor vehicle crash; Hx= history. Data are either formatted at mean ± standard deviation or median (interquartile range). *= Group main effect

S-Table 3: Mean Adjusted R^2 and standard deviation values between different implementations of geometric volume fractions and traditional DTI metrics in the entire HC sample only.

	NODDI		MDT	
	WM		WM	
Estimate	FA	MD	FA	MD
V_{ic}	0.26±0.001	0.29±0.007	0.47±0.004	0.21±0.002
V_{iso}	0.06±0.001	0.47±0.006	0.03±0.001	0.39±0.006
ODI	0.83±0.001	0.03±0.001	0.50±0.004	0.03±0.001
	GM		GM	
Estimate	FA	MD	FA	MD
V_{ic}	0.20±0.002	0.46±0.003	0.20±0.001	0.16±0.001
V_{iso}	0.03±0.002	0.56±0.005	0.03±0.001	0.43±0.004
ODI	0.72±0.002	0.02±0.001	0.21±0.002	0.04±0.000

Notes: NODDI = neurite orientation dispersion and density imaging; MDT = microstructure diffusion toolbox; WM = white matter; GM = grey matter; FA = fractional anisotropy; MD = mean diffusivity; V_{ic} = intracellular volume fraction; V_{iso} = isotropic volume fraction; ODI = orientation dispersion index.

S-Table 4: Mean Adjusted R^2 and standard deviation values between NODDI and MDT measures in the entire HC sample only.

		MDT					
		WM			GM		
NODDI	Estimate	V_{ic}	V_{iso}	ODI	V_{ic}	V_{iso}	ODI
	V_{ic}	***0.48±0.003***	0.36±0.007	0.01±0.001	**0.13±0.001**	0.32±0.003	0.05±0.004
	V_{iso}	0.19±0.001	**0.80±0.010**	0.01±0.000	0.06±0.001	**0.76±0.002**	0.06±0.000
	ODI	0.25±0.003	0.03±0.001	**0.66±0.007**	0.12±0.001	0.02±0.001	**0.29±0.003**

Notes: Bold numbers along diagonal indicated true measure-to-measure comparisons. WM = white matter; GM = grey matter; V_{ic} = intracellular volume fraction; V_{iso} = isotropic volume fraction; ODI = orientation dispersion index. Note that off-diagonal elements contain unique information due to the contrasting of the different volume fraction estimates from each model with each other.

S-Table 5: Results from models comparing dMRI and injury severity metrics

Wald-χ^2/p	FA (pmTBI>HC)	V_{ic} (pmTBI>HC)	GM V_{iso} (HC>pmTBI)	WM V_{iso} (pmTBI>HC)	ODI (pmTBI>HC)
5P	7.16/0.007	7.85/0.005	-	5.45/0.020	9.37/0.002
PCSI %	-	-	-	-	-
LOC	-	7.25/0.007	-	7.94/0.005	-
PTA	-	-	-	-	-
SRC	6.34/0.012	5.42/0.020	-	-	9.23/0.002
Complicated	-	-	-	-	8.66/0.003
pmTBI Hx	-	-	-	-	-

Notes: FA = fractional anisotropy; V_{ic} = intracellular volume fraction; V_{iso} = isotropic volume fraction; ODI = orientation diffusion index; pmTBI = paediatric mild traumatic brain injury; HC = healthy control; 5P = 5P Risk Score; PCSI = Post-Concussion Symptom Inventory (presented as percent of maximum score to account for age-related scale differences); LOC = duration of loss of consciousness; PTA = duration of post-traumatic amnesia; SRC = sport-related concussion vs. not (see S-Table 2); Complicated = complicated pmTBI as denoted by positive CT or structural MRI findings; Hx = history.

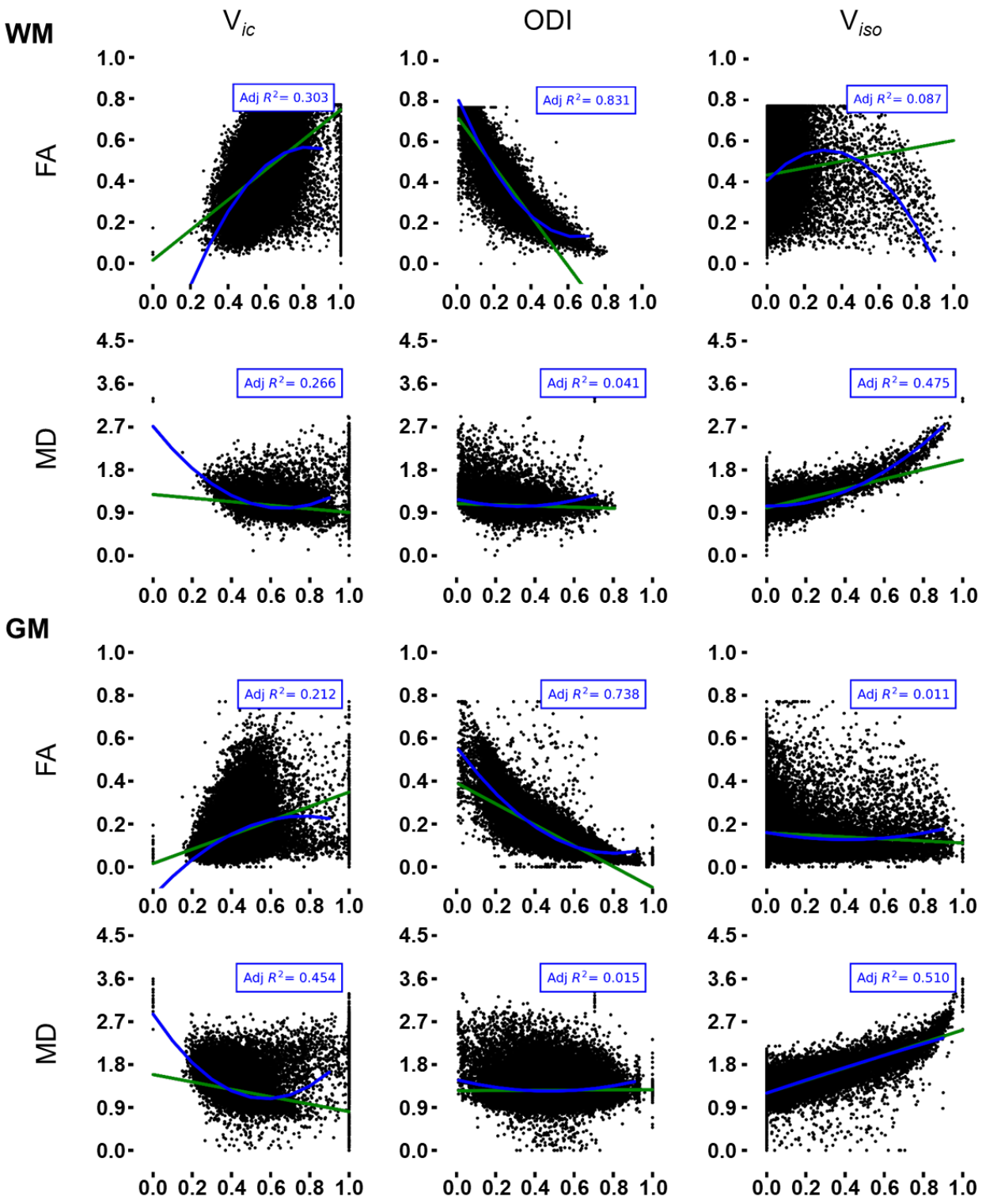

S-Figure 1: The scatterplots present relationships between microstructure estimates based on NODDI measures of cellular volume fractions (V_{ic}: intracellular volume fraction; V_{iso}: isotropic

volume fraction; ODI: orientation dispersion index) and DTI metrics (FA: fractional anisotropy; MD: mean diffusivity) separately for both white (WM) and grey (GM) matter. Data from each plot were randomly selected from a single healthy control in the study, with mean R^2 values presented for the entire sub-acute healthy control sample in S-Table 3. Data were modelled with either linear (green line) or linear and quadratic (blue line) terms. Adjusted R^2 (Adj R^2) values for each tissue type/metric are presented for the quadratic model.

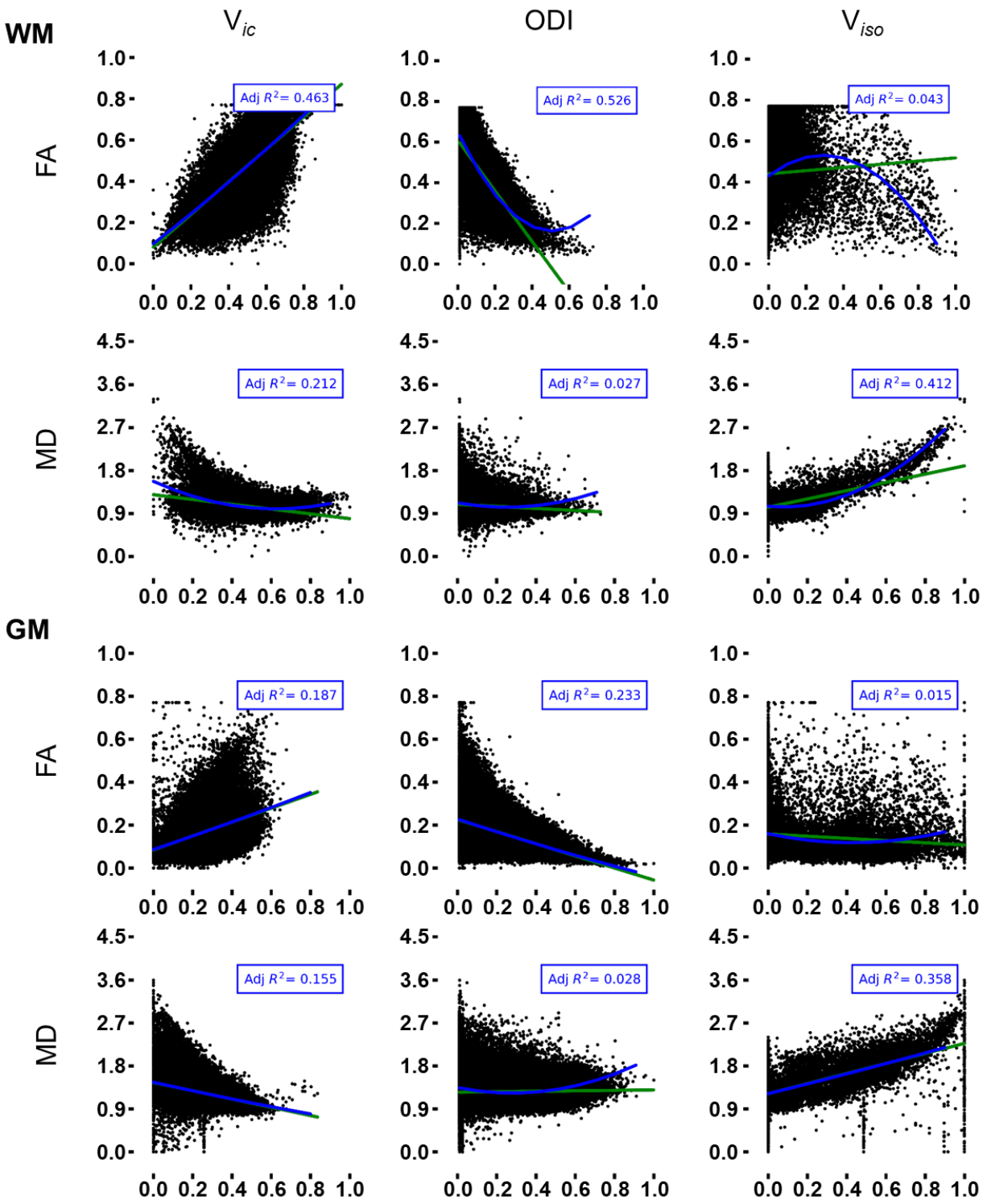

S-Figure 2: The scatterplots present relationships between microstructure estimates based on the biologically informed MDT estimates of cellular volume fractions (V_{ic}: intracellular volume fraction; V_{iso}: isotropic volume fraction; ODI: orientation dispersion index) and DTI metrics (FA:

fractional anisotropy; MD: mean diffusivity) separately for both white (WM) and grey (GM) matter. Data from each plot are presented for the same randomly selected healthy control for S-Figure 1, with mean R^2 values presented for the entire sub-acute healthy control sample presented in S-Table 3. Data were modelled with either linear (green line) or linear and quadratic (blue line) terms. Adjusted R^2 (Adj R^2) values for each tissue type/metric are presented for the quadratic model.

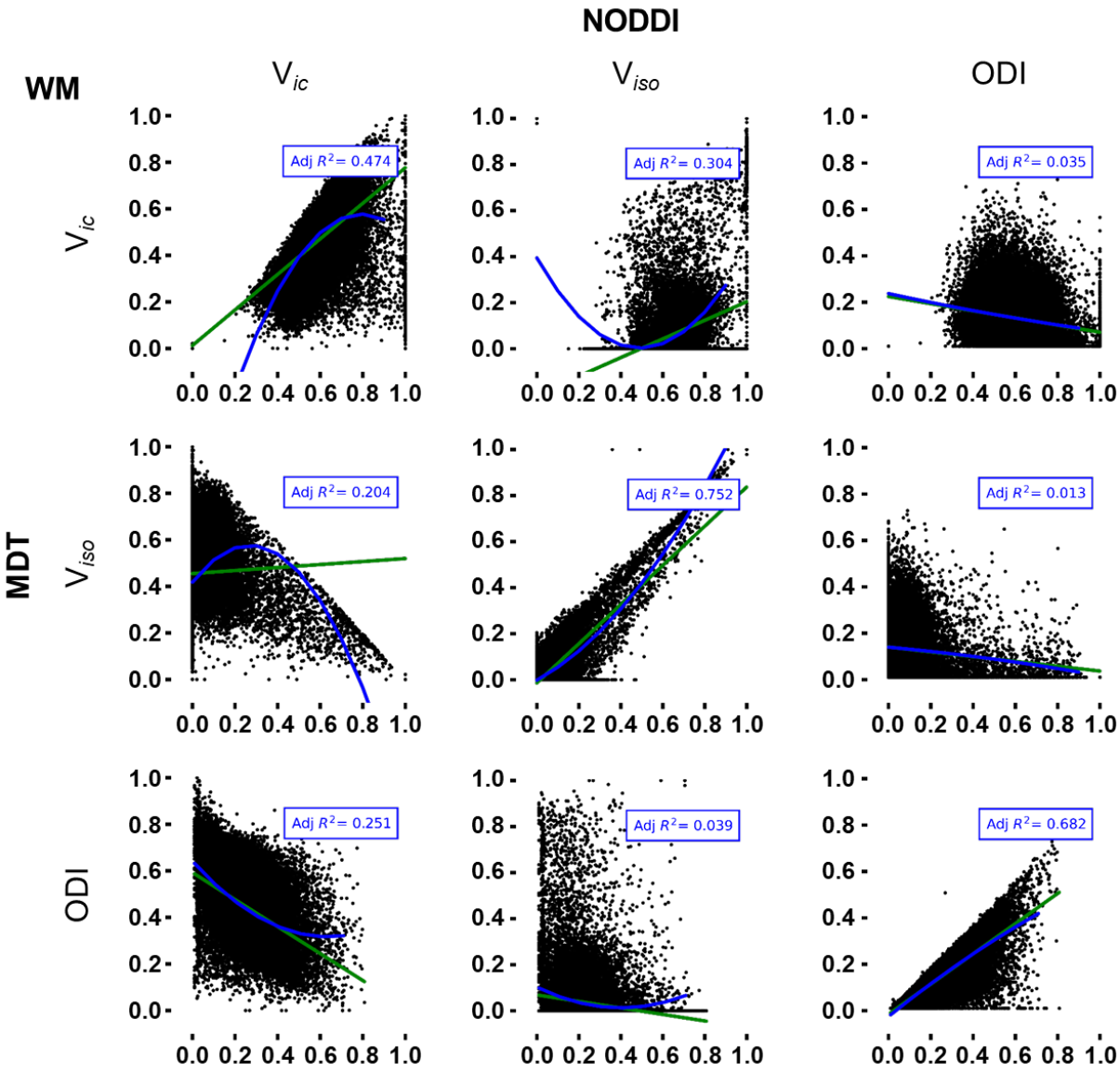

S-Figure 3: The scatterplots present relationships between microstructure estimates based on MDT and NODDI measures of cellular volume fractions (V_{ic}: intracellular volume fraction; V_{iso}: isotropic volume fraction; ODI: orientation dispersion index) for white matter (WM) only. Data from each plot are presented for the same randomly selected healthy control for S-Figure 1, with mean R^2 values presented for the entire sub-acute healthy control sample in S-Table 4. Data were modelled with either linear (green line) or linear and quadratic (blue line) terms. Adjusted R^2 (Adj R^2) values for each tissue type/metric are presented for the quadratic model.

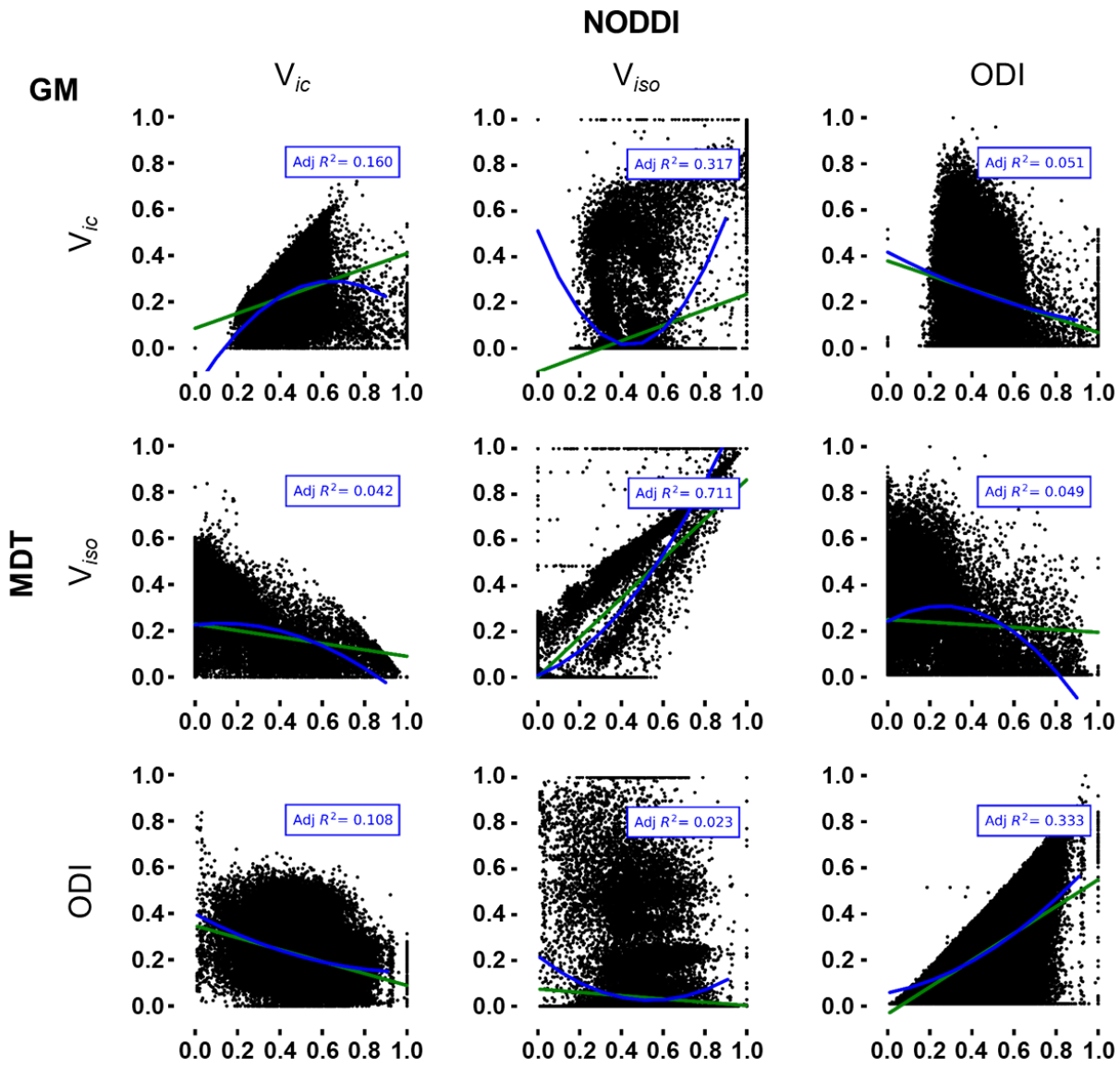

S-Figure 4: The scatterplots present relationships between microstructure estimates based on MDT and NODDI estimates of cellular volume fractions (V_{ic}: intracellular volume fraction; V_{iso}: isotropic volume fraction; ODI: orientation dispersion index) for grey matter (GM) only. Data from each plot are presented for the same randomly selected healthy control for S-Figure 1, with mean R^2 values presented for the entire sub-acute healthy control sample in S-Table 4. Data were modelled with either linear (green line) or linear and quadratic (blue line) terms. Adjusted R^2 (Adj R^2) values for each tissue type/metric are presented for the quadratic model.

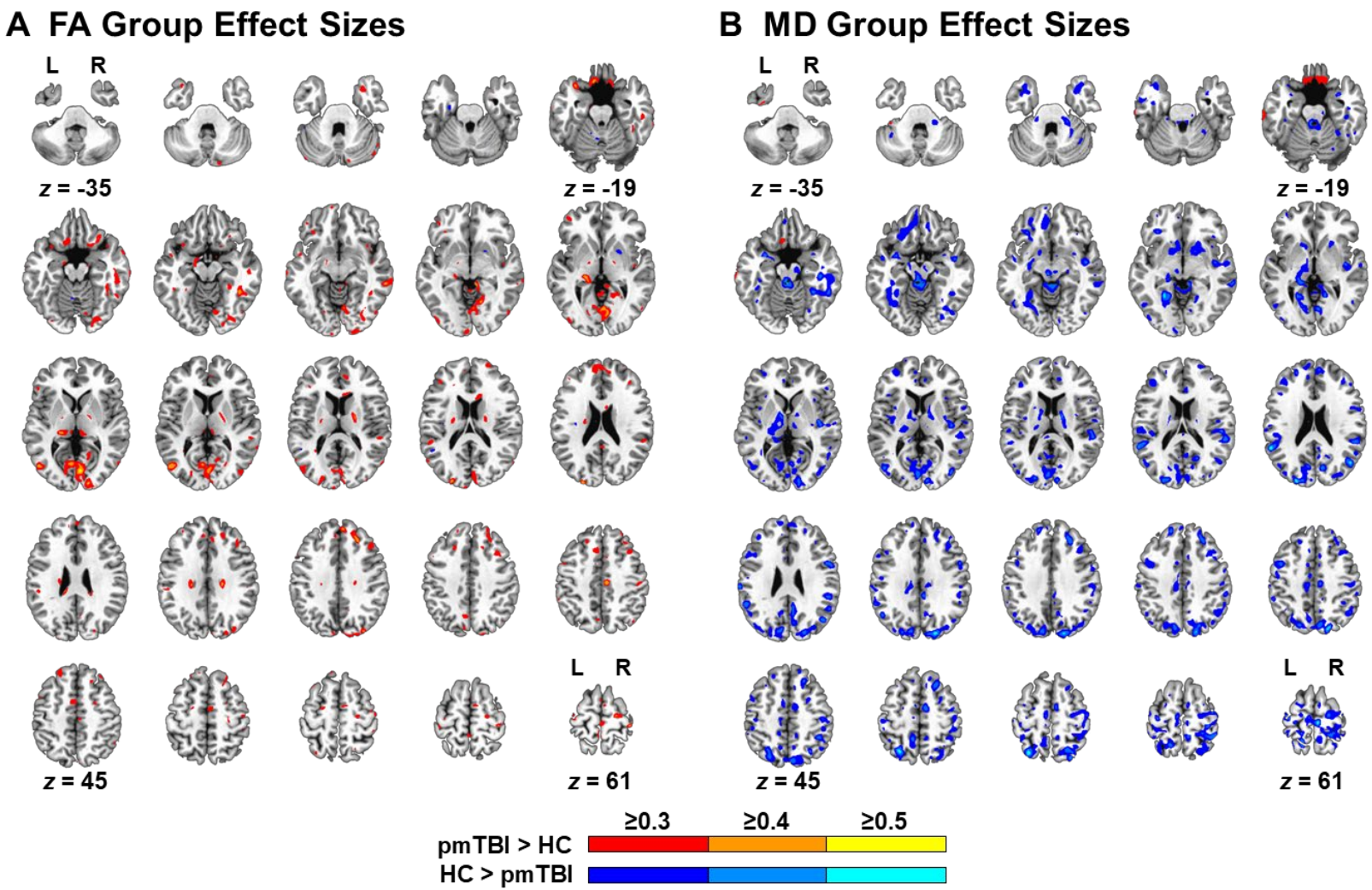

S-Figure 5: This figure displays brain areas showing small to moderate Cohen's *d* effect sizes for the main effect of Group for fractional anisotropy (FA; Panel A) and mean diffusivity (MD; Panel B) data. Regions with increased (pmTBI>HC) effect sizes appear in warm

colours (red: $d \geq 0.3$; orange: $d \geq 0.4$; yellow: $d \geq 0.5$), whereas regions with decreased (HC>pmTBI) effect sizes appear in cool colours (dark blue: $d \geq 0.3$; blue: $d \geq 0.4$; cyan: $d \geq 0.5$). Select axial (z) slices are displayed at 4 mm intervals according to the Talairach atlas with the left (L) and right (R) hemispheres denoted.

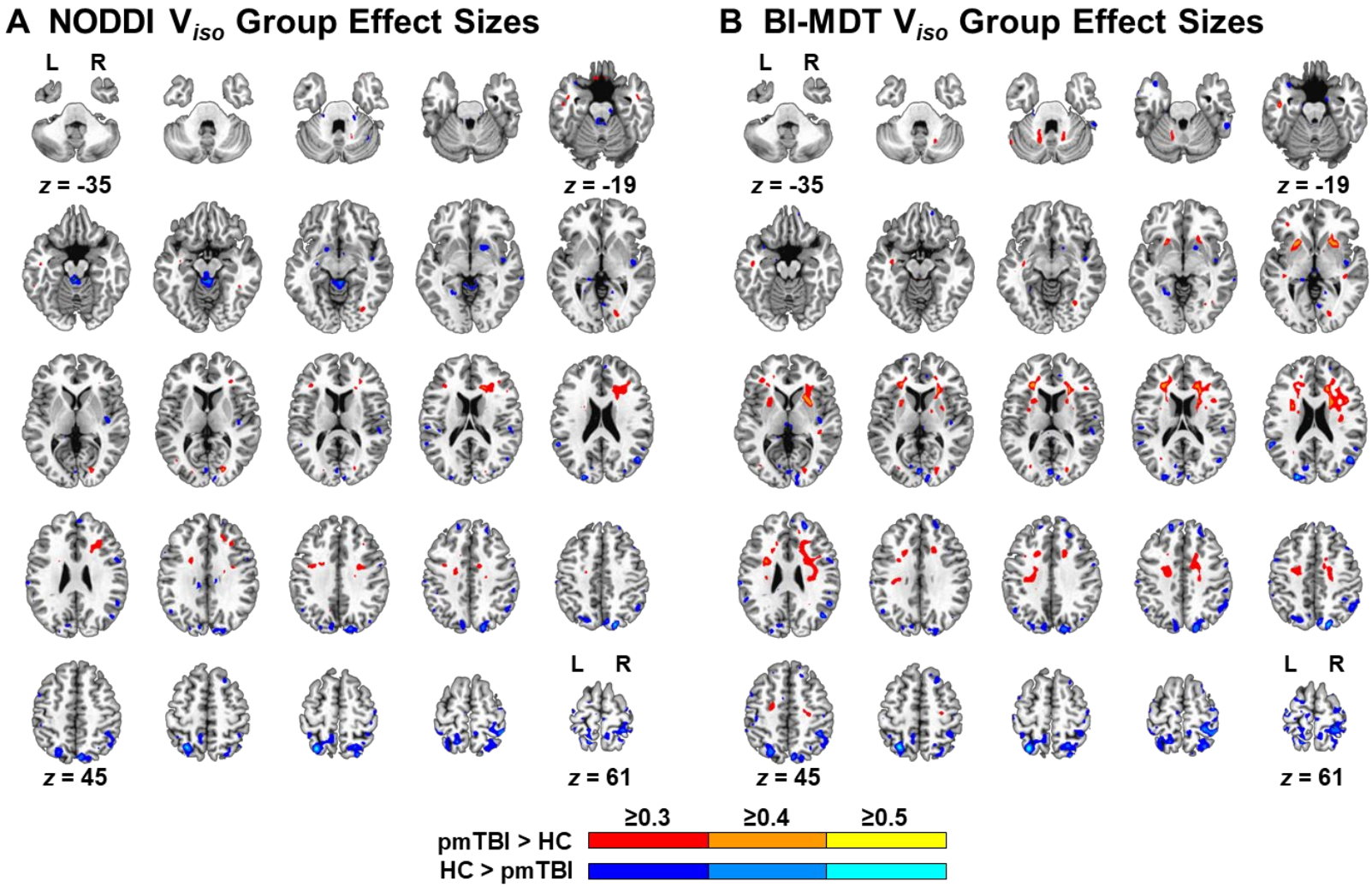

S-Figure 6: This figure displays brain areas showing small to moderate Cohen's *d* effect sizes for the main effect of Group for isotropic volume fraction (V_{iso}) derived using the Neurite Orientation Dispersion and Density Imaging algorithm (NODDI; Panel A) and using a

biologically informed Microstructure Diffusion Toolbox algorithm (BI-MDT; Panel B). Regions with increased (pmTBI>HC) effect sizes appear in warm colours (red: $d \geq 0.3$; orange: $d \geq 0.4$; yellow: $d \geq 0.5$), whereas regions with decreased (HC>pmTBI) effect sizes appear in cool colours (dark blue: $d \geq 0.3$; blue: $d \geq 0.4$; cyan: $d \geq 0.5$). Select axial (z) slices are displayed at 4 mm intervals according to the Talairach atlas with the left (L) and right (R) hemispheres denoted.

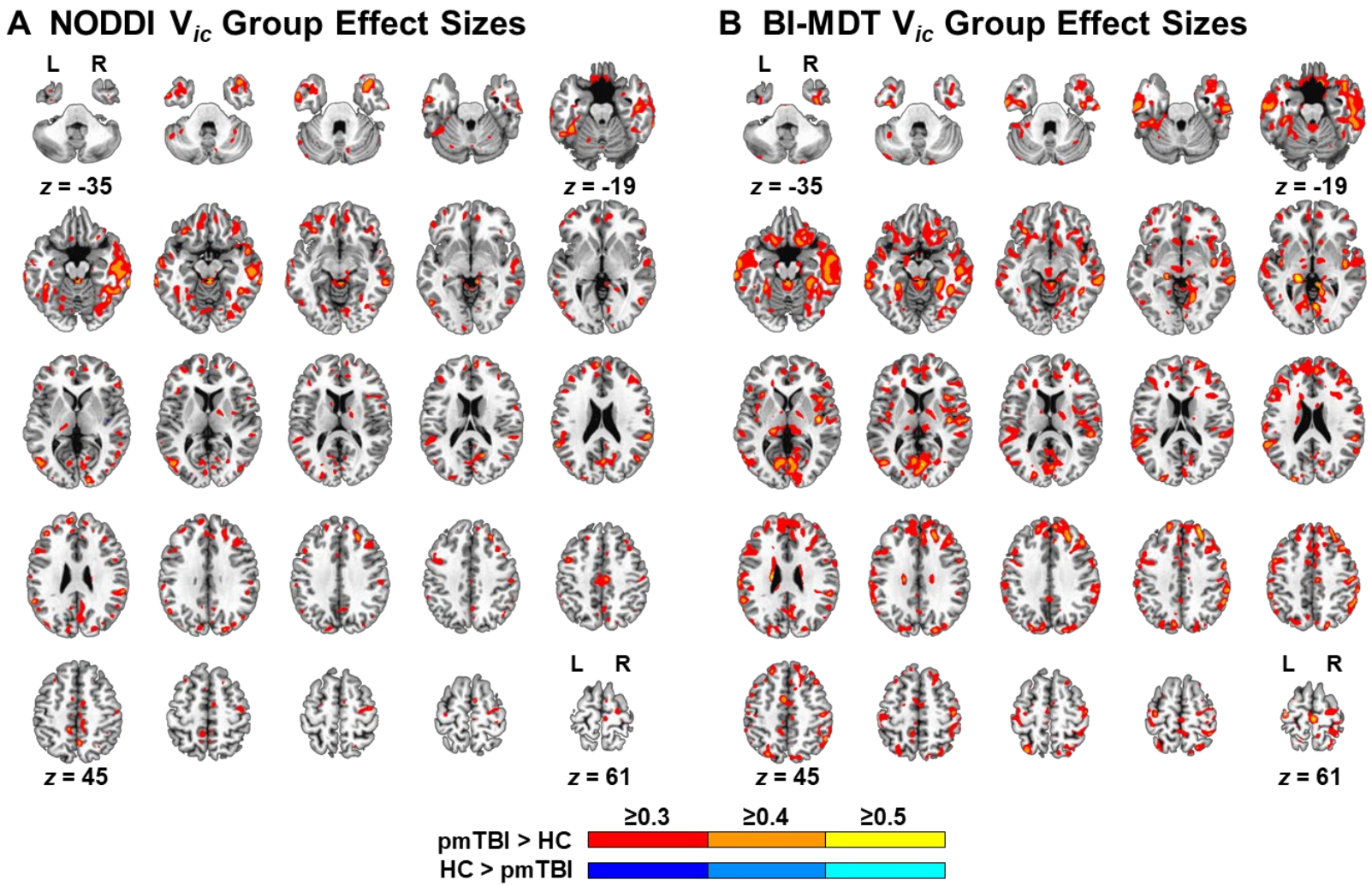

S-Figure 7: This figure displays brain areas showing small to moderate Cohen's *d* effect sizes for the main effect of Group for intracellular volume fraction (V_{ic}) derived using the Neurite Orientation Dispersion and Density Imaging algorithm (NODDI; Panel A)

and using a biologically informed Microstructure Diffusion Toolbox algorithm (BI-MDT; Panel B). Regions with increased (pmTBI>HC) effect sizes appear in warm colours (red: $d \geq 0.3$; orange: $d \geq 0.4$; yellow: $d \geq 0.5$), whereas regions with decreased (HC>pmTBI) effect sizes appear in cool colours (dark blue: $d \geq 0.3$; blue: $d \geq 0.4$; cyan: $d \geq 0.5$). Select axial (z) slices are displayed at 4 mm intervals according to the Talairach atlas with the left (L) and right (R) hemispheres denoted.

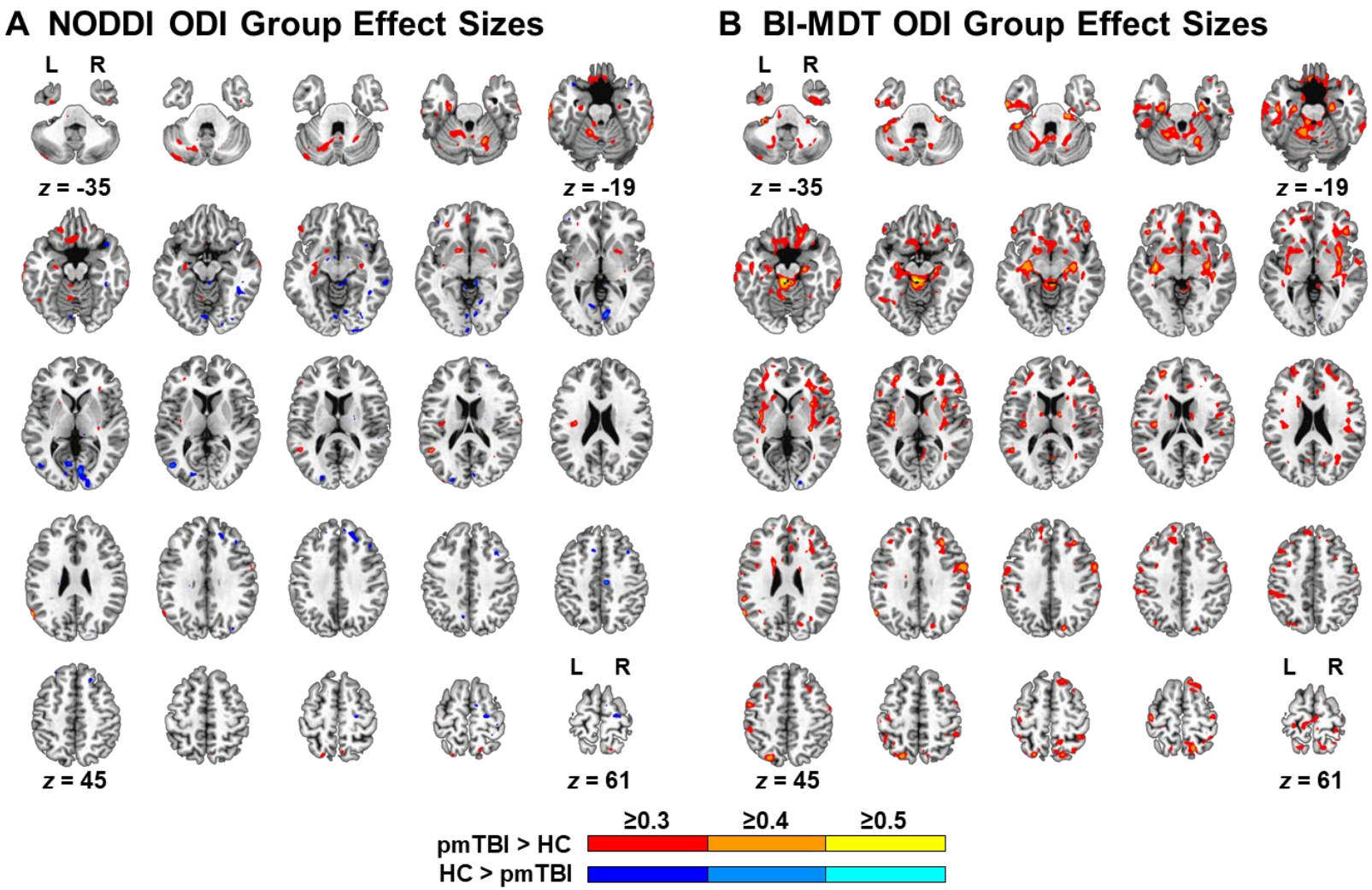

S-Figure 8: This figure displays brain areas showing small to moderate Cohen's *d* effect sizes for the main effect of Group for orientation dispersion index (ODI) derived using the Neurite Orientation Dispersion and Density Imaging algorithm (NODDI; Panel A) and using

a biologically informed Microstructure Diffusion Toolbox algorithm (BI-MDT; Panel B). Regions with increased (pmTBI>HC) effect sizes appear in warm colours (red: $d \geq 0.3$; orange: $d \geq 0.4$; yellow: $d \geq 0.5$), whereas regions with decreased (HC>pmTBI) effect sizes appear in cool colours (dark blue: $d \geq 0.3$; blue: $d \geq 0.4$; cyan: $d \geq 0.5$). Select axial (z) slices are displayed at 4 mm intervals according to the Talairach atlas with the left (L) and right (R) hemispheres denoted.

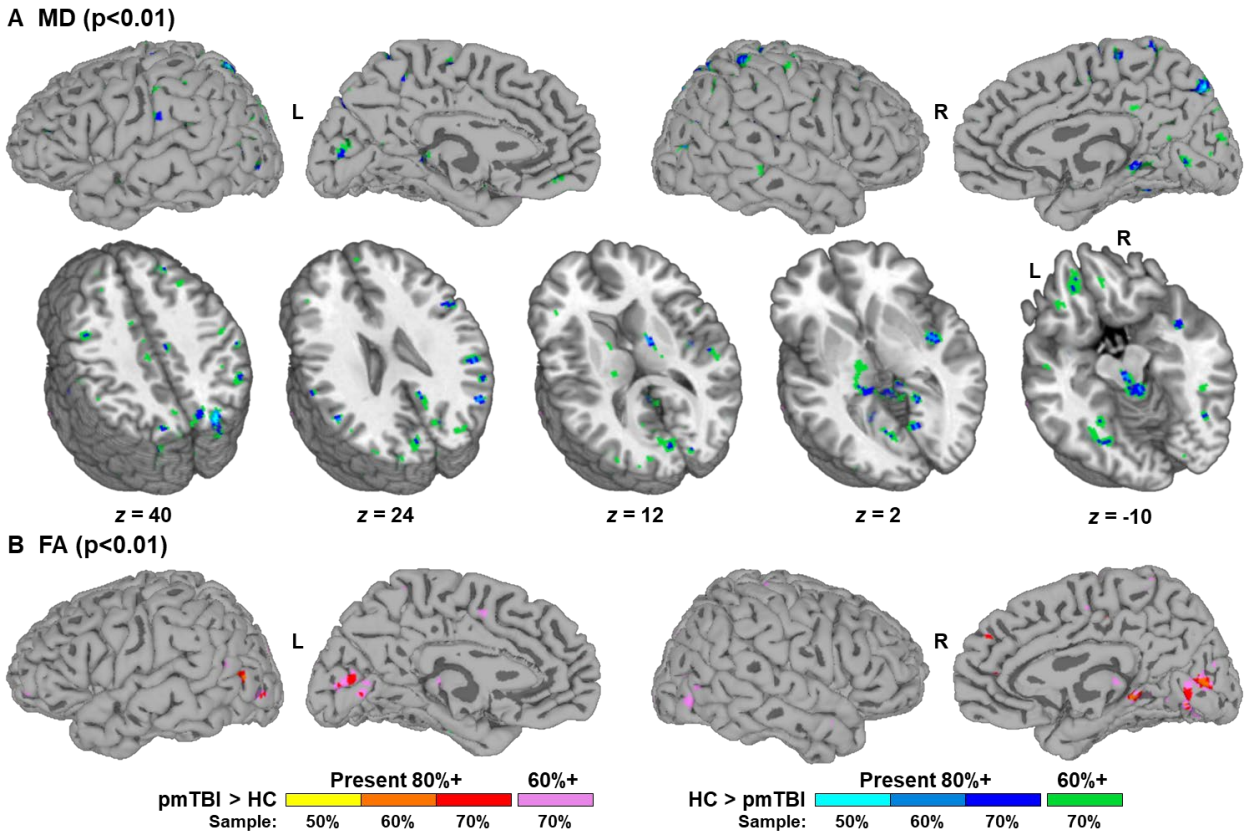

S-Figure 9: Results from cross-validation analyses of mean diffusivity (MD; Panels A) and fractional anisotropy (FA; Panels B) data at 50%, 60%, and 70% of the total sample size (sampled without replacement; 300 iterations). For each metric, a statistical threshold (uncorrected $p<0.01$) was applied to the main effect of Group for each iteration on a voxel-wise basis. Active voxels were then summed across iterations and divided by the number of iterations to form percentage values. Voxels demonstrating main effects are color-coded by both direction of effect (pmTBI>HC=warm; HC>pmTBI=cool) and level of reproducibility. In the first step, voxels were color-coded based for each sample size where a minimum of 80% reproducibility was achieved (50% of sample: yellow or cyan; 60% of sample: orange or middle blue; 70% of sample: red or dark blue). In the second step, voxels that achieved a minimum of 60% reproducibility at 70% of the total sample size were denoted (pink or green colours). Data are both projected to the surface

and displayed for selected axial slices (*z*; see Figure 2) according to the Talairach atlas for MD, whereas results are presented in projected format only for FA due to limited white matter and subcortical involvement. The majority of DTI findings indicated poor to moderate reproducibility when only 50% or 60% of the total sample was included in the analyses.

Appendix A: Code for MDT model.

```
#!/usr/bin/env python
# using MDT docs from here: https://mdt-toolbox.readthedocs.io/en/latest_release/mle_fitting.html

#
# 2) WM IC parallel at 1.7. EC estimated but less than this value with constraint
#   Model: "NODDI_Fixed_IC_EC_LT"; Outdir: " ic_1.7_ec_less"
#   The 7 parameters we will fit are: ['S0.s0', 'w_ic.w', 'NODDI_IC.theta', 'NODDI_IC.phi',
'NODDI_IC.kappa', 'w_ec.w', 'NODDI_EC.d']
#
# 4) GM IC parallel at 1.2. EC estimated with no constraint
#   Model: "NODDI_Fixed_IC_GT_Free_EC"; Outdir: " ic_1.2_ec_free"
#   The 7 parameters we will fit are: ['S0.s0', 'w_ic.w', 'NODDI_IC.theta', 'NODDI_IC.phi',
'NODDI_IC.kappa', 'w_ec.w', 'NODDI_EC.d']


import mdt

# Define alternative compartment models
from mdt import CompositeModelTemplate
from mdt.lib.post_processing import NODDIMeasures

class NODDI_Fixed_IC_EC_LT(CompositeModelTemplate):
   """ Fixed IC parallel. EC estimated but less than this value with constraint. """

   model_expression = '''
      S0 * ((Weight(w_csf) * Ball) +
           (Weight(w_ic) * NODDI_IC) +
           (Weight(w_ec) * NODDI_EC))
   '''

   # initialize the diffusivity to something lower then 1.7e-9 (the default)
   # to prevent the optimization routine from starting on an edge defined by your constraint
   inits = {
      'NODDI_EC.d': 1.6e-9
   }

   fixes = {
         'NODDI_IC.d': 1.7e-9,
         'Ball.d': 3.0e-9,
         'NODDI_EC.dperp0': 'NODDI_EC.d * w_ec.w / (w_ec.w + w_ic.w)',
         'NODDI_EC.kappa': 'NODDI_IC.kappa',
         'NODDI_EC.theta': 'NODDI_IC.theta',
         'NODDI_EC.phi': 'NODDI_IC.phi'}
```

```
    constraints = '''
        constraints[0] = NODDI_EC.d - NODDI_IC.d;
    '''
    extra_optimization_maps = [NODDIMeasures.noddi_watson_extra_optimization_maps]
    extra_sampling_maps = [NODDIMeasures.noddi_watson_extra_sampling_maps]




class NODDI_Fixed_IC_EC_Free(CompositeModelTemplate):
    """ Fixed IC parallel. EC estimated with no constraint. """

    model_expression = '''
        S0 * ((Weight(w_csf) * Ball) +
              (Weight(w_ic) * NODDI_IC) +
              (Weight(w_ec) * NODDI_EC))
    '''

    fixes = {
            'NODDI_IC.d': 1.2e-9,
            'Ball.d': 3.0e-9,
            'NODDI_EC.dperp0': 'NODDI_EC.d * w_ec.w / (w_ec.w + w_ic.w)',
            'NODDI_EC.kappa': 'NODDI_IC.kappa',
            'NODDI_EC.theta': 'NODDI_IC.theta',
            'NODDI_EC.phi': 'NODDI_IC.phi'}


    extra_optimization_maps = [NODDIMeasures.noddi_watson_extra_optimization_maps]
    extra_sampling_maps = [NODDIMeasures.noddi_watson_extra_sampling_maps]

    mdt_file = 'mdt.prtcl'

    protocol = mdt.create_protocol(
            bvecs='dwi.concat.edc.eddy_rotated_bvecs',
            bvals='dwi.concat.bvals',
            out_file=mdt_file)

    input_data = mdt.load_input_data(
        'dwi.concat.edc.nii.gz',
        mdt_file,
        'dwi.concat.edc.mask.nii.gz'
    )



        ########################
        #   WM IC parallel at 1.7. EC estimated but less than this value with constraint.
        ########################
```

```
# model reference
model_name = 'NODDI_Fixed_IC_EC_LT'
# results dir
output_dir = ' ic_1.7_ec_lt'
# file check
   # initialize model
   inits = mdt.get_optimization_inits(model_name,
                              input_data,
                              output_dir,
                              cl_device_ind=[0,1],
                              method='Powell'
                              )

   # fit model
   mdt.fit_model(model_name,
              input_data,
              output_dir,
              initialization_data={'inits': inits},
              use_cascaded_inits=True,
              method='Powell',
              optimizer_options={'patience': 2},
              cl_device_ind=[0,1],
              tmp_results_dir='/tmp'
              )



######################
#   GM IC parallel at 1.2. EC estimated with no constraint
######################
# model reference
model_name = 'NODDI_Fixed_IC_EC_Free'
# results dir
output_dir = 'ic_1.2_ec_free'

   # initialize model
   inits = mdt.get_optimization_inits(model_name,
                              input_data,
                              output_dir,
                              cl_device_ind=[0,1],
                              method='Powell'
                              )

   # fit model
   mdt.fit_model(model_name,
              input_data,
              output_dir,
              initialization_data={'inits': inits},
```

```
use_cascaded_inits=True,
method='Powell',
optimizer_options={'patience': 2},
cl_device_ind=[0,1],
tmp_results_dir='/tmp'
)
```